Hindawi
Applied Bionics and Biomechanics
Volume 2024, Article ID 8369544, 12 pages
https://doi.org/10.1155/2024/8369544

Research Article

Electromechanical Coupling Model for Ionic Liquid Gel Soft Actuators

Chenghong Zhang,[1,2] **Chengguang Zhang**,[3] **Guangping Tian**,[4] **and Xun Gu**[2]

[1]*Key Laboratory of Advanced Manufacturing Technology, Ministry of Education, Guizhou University, Guiyang 550025, Guizhou, China*
[2]*School of Electronics and Information Engineering, Guiyang University, Guiyang 550005, Guizhou, China*
[3]*School of Mechanical and Electrical Engineering, Zhoukou Normal University, Zhoukou 466001, Henan, China*
[4]*State-Owned Jinjiang Machinery Factory, Chengdu 610043, Sichuan, China*

Correspondence should be addressed to Chenghong Zhang; zhangchenghong@gyu.cn

Received 7 October 2023; Revised 23 December 2023; Accepted 18 January 2024; Published 13 February 2024

Academic Editor: Liwei Shi

A soft robot is composed of soft materials, which exhibit continuous deformation and driving structure integration and can arbitrarily change shapes and sizes over wide ranges. It shows strong adaptability to unstructured environments and has broad application prospects in military reconnaissance, medical rescues, agricultural production, etc. Soft robots based on ionic electroactive polymers (EAPs) have low-driving voltages, large-actuation displacements, fast responses, light weights, and low powers and have become a hot research field of bionic robots. Ionic liquid gels (ILGs) are new ionic EAPs. In this study, a new soft actuator was designed based on an ILG, and the electromechanical coupling model of an ILG soft actuator was studied in detail. Based on the system transfer function method, a mechatronic coupling model for the soft actuator was developed. According to the material characteristics and current response law of the ILG-containing EAP, an equivalent circuit model was used to describe transfer of the output current and input voltage. Based on the equivalent transformer model for ionic polymer–metal composite (IPMC) actuators proposed by Claudia Bonomo, the electromechanical coupling equation and a driving equation of the ILG soft actuator were established. The least-squares method was used with the coupling model of an ILG soft actuator to identify the system parameters for the model, and the effects of the structural parameters on the end displacement and driving force of the soft actuator were analyzed.

1. Introduction

The ionic liquid gel (ILG) is a new soft robot actuator flexible material developed in this study, which contains two components: a polymer and an ionic liquid. The ILG mixed solution consisted of four raw materials, namely, 1-butyl-3-methylimidazolium tetrafluoroborate ($BMIMBF_4$), hydroxyethyl methacrylate (HEMA), 2-diethoxyacetophenone (DEAP), and TiO_2. Under ultraviolet (UV) lamps, they polymerized to form polymeric gels [1–3]. The traditional flexibility mechanism uses the elastic deformations of flexible materials to transmit or convert motion, force, or energy [4, 5]. It requires an external driving source during the working process, thereby changing the kinematic body of the flexible mechanism. A soft robot is a special flexible mechanism, and the soft robot itself has active deformation ability. Its actuator provides the driving function and structural function [6–8].

Electrolytes are important parts of ionic electroactive polymer (EAP) soft actuators. The traditional electrolyte solutions have been replaced with ionic liquids, and the ionic liquid polymeric gel prepared by the ionic liquid loading method constitutes a new ionic EAP. The ionic liquid polymer gels used to make ionic EAP soft actuators require high ionic conductivities, good electrochemical stabilities, and high mechanical strengths [9, 10].

For soft actuator systems, the general input signals are the excitation voltage and current, and the output signals can be current, displacement, speed, driving force, etc. [11, 12]. The ILG is a new ionic EAP material, and the conductivity mechanism is not exactly the same as those of traditional ionic EAPs. The response of the actuator under the action

of the applied electric field is essentially caused by the simultaneous migration of anions and cations. The bending deformations of the ILG soft actuator in response to an applied voltage is a complex electrical–chemical–mechanical coupling process.

At present, the research on ionic EAP soft actuators is mainly focused on traditional materials such as ionic polymer–metal composite (IPMC) [13, 14]. For traditional ionic EAPs, scholars have used equivalent circuit models and electromechanical coupling models to describe their current responses, displacement responses, and output driving forces, respectively [15]. However, there are very few research models for ILG soft actuators. Therefore, to understand the electrical excitation responses of ILG soft actuators, the equivalent circuit model and electromechanical coupling model of ILG actuators were derived and a complete modeling method proposed.

The actuator model consists of three parts: the equivalent circuit model, the equivalent transformer model, and the cantilever model. The equivalent circuit model of the actuator is derived by drawing on supercapacitor modeling theory, and the function is to convert the input voltage of the actuator into the driving current. The function of the equivalent transformer model is to map the charge to the induced stress of the actuator due to the bending deformation. The function of the cantilever beam model is to convert the induced stress of the electrode into the equivalent force moment, which is then reflected as the end displacement of the actuator. The equivalent transformer model and the cantilever beam model constitute the electromechanical coupling model of the soft actuator. The influence of the geometry/material characteristic parameters of the actuator on the end displacement is described, and the corresponding relationship between the input and output variables of the system is established to form a complete model for the end displacement or equivalent moment for the ILG actuator controlled by the input voltage.

2. Design of Soft Robots Based on ILGs

As a typical soft condensed matter, ILG gels contain porous polymer chains and many small molecules. They have the self-binding characteristics of general solids on the macroscopic level and the free flow characteristics of general fluids at the microscopic level, so they exhibit many complex properties and mechanical properties that are completely different from those of traditional materials [16]. ILGs contain free-flowing ionic liquids, which are high-performance ionic EAPs with many excellent characteristics, such as large-deformation ranges, rapid responses, low-power consumption, light weights, and high stabilities. ILG materials can be processed by hot pressing, light curing, and other methods. Because of their unique response properties, they have very broad application prospects in the soft robots.

ILG soft actuators have five-layer structures, as shown in Figure 1. They are similar to the structures of traditional electroactive polymer actuators and are symmetrical [17]. The intermediate layer is an electroactive polymer composed of the ILG, which is used to store the ionic liquid. A soft actuator electrode layer composed of activated carbon on both sides is covered on the outside of the middle layer and is used to store anions and cations. Due to the characteristics of activated carbon, such as a high-specific surface area, high conductivity, high density, and strong adsorption force, it is a suitable electrode material for the soft actuators. A gold foil is used as a current collector and pasted on the outer surface of the activated carbon layer. When the actuator is working, one end of the wire is connected to the metal outside the soft actuator. The wire is led out of the external electrode, and the other end is connected to the drive power supply. The soft actuator can be fixed by a cantilever beam or stood vertically.

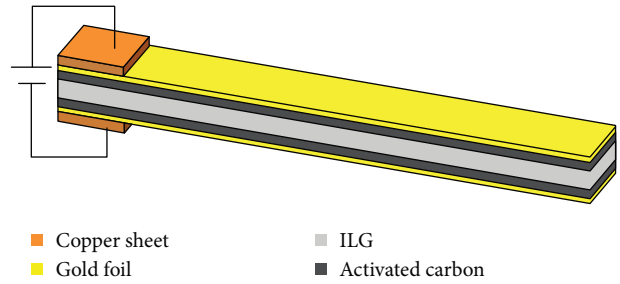

Figure 1: The five-layer structure of the soft actuator.

The ILG soft actuator shown in Figure 2 has an ionic liquid polymer gel layer, active carbon layer, and gold foil layer with sizes of 30 mm × 5 mm. Figure 2(a) shows an ILG sample with a thin layer of $BMIMBF_4$ covering the gel surface due to osmosis. Since ionic liquids are viscous, the activated carbon electrode can be fixed directly on the outside of the gel, pressed under a tablet press at 1 N for 5 min, and then put into an oven at 60°C to dry for 10 min, as shown in Figure 2(b). Finally, the gold foil is evenly pasted on the surface of the activated carbon layer to obtain an ILG soft actuator, as shown in Figure 2(c).

3. ILG Soft Actuator Equivalent Circuit Model

3.1. ILG Actuator Equivalent Circuit Model. ILGs are ideal materials for the preparation of supercapacitors [18]. The equivalent circuit of an ILG actuator is based on supercapacitor theory, and the current responses of robot actuators are systematically analyzed. As with IPMC materials, conduction by the ILG soft actuators can also be summarized as a combination of ion current, displacement current, and electronic current. However, the principle for generating the ion current is different: the ion current of the IPMC is formed by directional movement of hydrated cations, while the ion current of the ILG is formed by simultaneous movement of anions and cations in the opposite directions. Since, the ion current and displacement current change dynamically with time and it is impossible to measure and analyze them individually, the ion current and displacement current are synthesized and placed in a branch to characterize their dynamic characteristics in the entire actuator.

Usually, the electronic current response of an IPMC actuator is nonlinear at the initial stage. However, because the response speed of the electronic current in the ILG

(a) (b) (c)

Figure 2: Assembly process of the soft actuator; (a) the ILG; (b) the activated carbon layer is affixed; and (c) the gold foil layer is affixed.

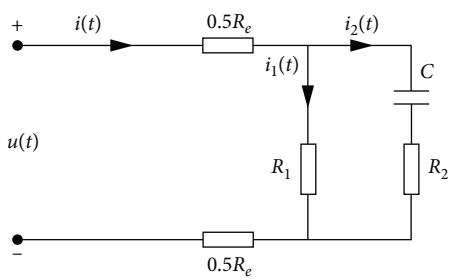

Figure 3: First-order equivalent circuit model of the soft actuator.

actuator is much faster than the ion current response, the on voltage of the diode is very low, the voltage applied by the robot actuator is much greater than the on voltage of the diode, and the initial transient process of the electronic current is negligible compared to the ion current. Ignoring the nonlinearity of the electronic current, the value of the electronic current passing through the actuator is constant, and a pure resistance branch is used to model the steady-state characteristics throughout the actuator.

Therefore, the current response of an ILG soft actuator is mainly composed of ion current and electron current, which are manifested as ion current in the dynamic state and the electronic current in the static state. Since, the viscosities of ionic liquids are greater than those of aqueous solutions, the current response is slower than that of the IPMC.

The first-order equivalent circuit model of the ILG soft actuator is a lumped parameter model [19], as shown in Figure 3, and its structure is similar to the classical equivalent circuit model for supercapacitors. R_1 is the DC equivalent resistance of the actuator, which represents the electronic current branch and reflects the static characteristics of the current response; R_2 is the AC equivalent resistance of the actuator; C is the equivalent capacitance of the actuator, which represents the ion current branch and reflects the dynamic characteristics of the actuator; and R_e is the surface electrode resistance of the actuator.

As shown in Figure 3, the first-order equivalent circuit model is represented by the following equations:

$$\begin{cases} i_1(t) = \dfrac{u_{\mathrm{RC}}(t)}{R_1} \\ R_2 i_2(t) + \dfrac{1}{C}\displaystyle\int i_2(t)dt = u_{\mathrm{RC}}(t)\,, \\ i(t) = i_1(t) + i_2(t) \\ u_{\mathrm{RC}}(t) + i(t)R_e = u(t) \end{cases} \tag{1}$$

where i_1 is the electronic current of the actuator, i_2 is the ion current of the actuator, i is the input current of the actuator, u is the input voltage, and u_{RC} is the actuator voltage.

With zero input, the Laplace transform of Equation (1) is performed; then, the transfer function of the output current and input voltage of the robot actuator can be written as follows:

$$\begin{aligned} \frac{I(s)}{U(s)} &= \frac{(R_1+R_2)Cs+1}{[R_1R_2+R_e(R_1+R_2)]Cs+R_1+R_e} \\ &= \frac{R_1+R_2}{R_1R_2+R_e(R_1+R_2)} - \frac{{R_1}^2}{[R_1R_2+R_e(R_1+R_2)]^2C} \\ &\quad \cdot \frac{1}{s+\frac{R_1+R_e}{[R_1R_2+R_e(R_1+R_2)]C}}. \end{aligned} \tag{2}$$

When a step signal with an amplitude of U is input, Equation (2) has the following form:

$$\begin{aligned} I(s) &= \frac{(R_1+R_2)Cs+1}{[R_1R_2+R_e(R_1+R_2)]Cs+R_1+R_e} \cdot \frac{U}{s} \\ &= \frac{R_1R_2+R_1R_e+R_2R_e}{[R_1R_2+R_e(R_1+R_2)](R_1+R_e)} \cdot \frac{U}{s} \\ &\quad + \frac{{R_1}^2}{[R_1R_2+R_e(R_1+R_2)](R_1+R_e)} \\ &\quad \times \frac{U}{s+\frac{R_1+R_e}{[R_1R_2+R_e(R_1+R_2)]C}} \end{aligned}. \tag{3}$$

The inverse Laplace transform is performed on both sides of Equation (3); then,

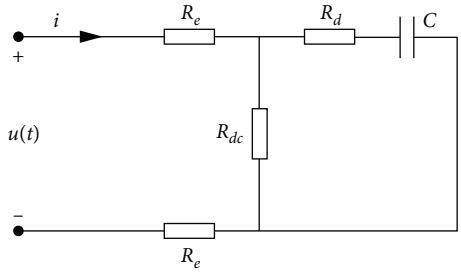

Figure 4: Simplified *R–C* equivalent circuit model of the soft actuator.

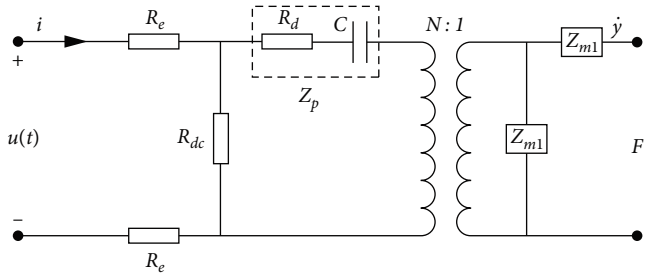

Figure 5: Equivalent model of an electromechanical coupling transformer for a soft actuator.

$$i(t) = a_0 + a_1 e^{-\lambda t}, \tag{4}$$

where

$$\begin{cases} a_0 = U_0 \dfrac{R_1R_2 + R_1R_e + R_2R_2}{[R_1R_2 + R_e(R_1 + R_2)](R_1 + R_e)} \\ a_1 = U_0 \dfrac{R_1^2}{[R_1R_2 + R_e(R_1 + R_2)](R_1 + R_e)}. \\ \lambda = \dfrac{R_1 + R_e}{[R_1R_2 + R_e(R_1 + R_2)]C} \end{cases} \tag{5}$$

Equation (4) shows that equivalent circuit modeling of ILG robot actuators with first-order circuit models has the advantages of a simple structure and easy parameter identification, so it is suitable for the design and analyses of the soft actuators.

3.2. Equivalent Transformer Model for Electromechanical Coupling of Actuators. Assuming reasonable equivalence, the equivalent circuit is one of the methods used to analyze electromechanical coupling, and the components in the circuit have clear physical meanings, which describe the states of the intermediate variables of the system simplify the analysis.

In this section, a linear transformer equivalent circuit model (the gray box model was established to describe the electromechanical coupling relationships of ILG actuators, and combined with the Laplace transform, the relationships between the input and output variables of the system will be derived by considering the structural parameters of the actuator itself. The simplified *R–C* equivalent circuit model of the ILG actuator is shown in Figure 4, and the equivalent model of the electromechanical coupling transformer in the ILG actuator is shown in Figure 5.

Among them, Re_1 and Re_2 represent the resistances of the metal layers in the upper and lower plates of the actuator, R_{dc} is the DC steady-state equivalent resistance of the actuator, C is the actuator capacitance, and R_d is the dynamic equivalent resistance. The *R–C* equivalent circuit model in Figure 4 is replaced by the electrical parameters in the Newbury transformer circuit model to obtain the electromechanical coupling equivalent model of a soft actuator shown in Figure 5, where the left half of the transformer shows the electrical parameters and the right half represents the mechanical

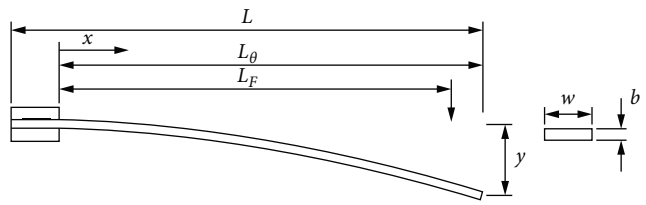

Figure 6: Schematic diagram of the cantilever beam model for the soft actuator.

parameters. The variables u and i represent the voltage and current of an ILG soft actuator, F is the external force on the actuator, and $\dot{y}$ is the speed of the driver under the action of external force.

3.2.1. Electromechanical Coupling Equations. As with the equivalent circuit models of ion polymer sensors, coupling between the mechanical and electrical properties is modeled with linear coupling equations, and the input–output relationship of a soft actuator is established for the cantilever beam bending deformation model. In mathematical modeling of the mechatronic coupling, it is assumed that the variables in the electrical and mechanical domains are linearly coupled. The energy transition between the two domains can be generated through changes in the system state variables.

It is helpful to model electromechanical transducers with the equivalent circuit models because it provides a graphical representation of the controlling equations for electromechanical systems. Each circuit element has a clear physical meaning, and users can examine the relationships between the various elements without being forced to study the fundamental equations. While only linear circuits are considered in electromechanical coupling analyses, Laplace domain circuit analysis provides a straightforward way to obtain the relationships between any system variables. Linear coupling between the electrical and mechanical domains can be represented with an ideal linear transformer model, as shown in Figure 5.

Ignoring the influence of gravity on the soft actuator, it was simplified to a cantilever beam type actuator, and its structural parameters are shown in Figure 6. When analyzing a bending deformation of the actuator, the axis of the actuator before deformation is the x-axis, the vertical downwards direction is the y-axis, the total length of the actuator is L, the length of the free end is L_0, the width is w, and the thickness

is b. According to the Euler–Bernoulli beam theory, shear deformation can be omitted for slender beams; that is, it is assumed that the actuator has only a bending deformation and is completely rigid for actuator deformation.

The mechanical impedance caused by the stiffness of an ILG soft actuator is represented by Z_{m1} in Figure 5. In Figure 6, the bending moment resulting from the load f applied by the actuator at the distance L_F from the support end is as follows:

$$M = F(L_F - x), \tag{6}$$

where x is the distance from the fixed end along the bending direction of the beam. For small deflections, the relationship between the actuator moment and deflection is as follows:

$$\frac{M}{\mathrm{EI}} = \frac{d^2y}{dx^2}, \tag{7}$$

where E is Young's (elastic) modulus, and I is the moment of inertia for the cross-section of the actuator.

The moment of inertia of the actuator cross-section is as follows:

$$I = \int_A y^2 dA = \int_{-\frac{b}{2}}^{\frac{b}{2}} y^2 \mathrm{wdy} = \frac{\mathrm{wb}^3}{12}. \tag{8}$$

Combined with the boundary conditions for the cantilever beam ($u\,(x=0)=0$ and $\frac{du}{dx}\,(x=0)=0$), the area moment of inertia is written based on the width w and thickness b of the actuator, and the expression at $x=L_F$ is as follows:

$$y = \frac{4FL_F^3}{Ewb^3}. \tag{9}$$

To obtain the Laplace domain expression of Z_{m1}, which expresses the force exceeding the velocity (much lower than the resonance), the Laplace transform on Equation (9) was performed and solved for Z_{m1}.

$$Z_{m1} = \frac{1}{s}\frac{Ewb^3}{4L_F^3}. \tag{10}$$

Z_{m2} is an inertial term, and the purpose of adding Z_{m2} to the model is to extend the effective frequency range of the actuator, which improves the accuracy of the model near the first-order natural frequency. The expression of Z_{m2} in the Laplace domain is [20] as follows:

$$Z_{m2} = s\frac{3L_0^4\rho_m wb}{L_F^3\Gamma^4}, \tag{11}$$

where Γ is the first-order natural frequency and ρ_m is the density of the soft actuator.

In the equivalent circuit model in Figure 5, the electrical impedance of the ILG soft actuator was represented by two terms; R_{dc} is the DC resistance and Z_p simulates the actuator's ability to store charge. To simplify the expression of R_{dc} and Z_p, the ILG soft actuator is considered a homogeneous material with fully conductive electrodes on both surfaces.

The DC equivalent resistance of a soft actuator can be expressed as as follows:

$$R_{dc} = \rho_{dc} \cdot \frac{b}{Lw}, \tag{12}$$

where ρ_{dc} represents the DC equivalent resistivity and L represents the total length of the actuator, including the fixed terminal. The electrical impedances of ILG soft actuators show high resistance with DC currents, small resistances with high frequency currents, and high capacitance at medium frequency. Similarly, R_{e1}, R_{e2}, and R_d can all be expressed with similar Equation (12) as follows:

$$\begin{cases} R_{e1} = \rho_{e1} \cdot \dfrac{b_{e1}}{\mathrm{Lw}} \\ R_{e2} = \rho_{e2} \cdot \dfrac{b_{e2}}{\mathrm{Lw}}, \\ R_d = \rho_d \cdot \dfrac{b}{\mathrm{Lw}} \end{cases} \tag{13}$$

where ρ_{e1}, ρ_{e2}, and ρ_d are the resistivity of the upper and lower metal electrode plates of the actuator and the dynamic equivalent resistivity of the actuator, respectively, and b_{e1} and b_{e2} are the thicknesses of the upper and lower electrode plates, respectively.

For parallel plate capacitors, the expression for capacitance C is as follows:

$$C = \varepsilon \cdot \frac{Lw}{b}, \tag{14}$$

where ε is the equivalent permittivity of the material between the two electrode plates.

The expression for the impedance Z_p in the circuit of Figure 5 in the Laplace domain is as follows:

$$Z_p = R_d + \frac{1}{Cs}. \tag{15}$$

Substituting Equations (13) and (14) into Equation (15) yields as follows:

$$Z_p = \frac{b}{Lws} \cdot \left(\rho_d s + \frac{1}{\varepsilon}\right) = \frac{1}{\frac{Lws}{b} \cdot \frac{\varepsilon}{(\rho_d \varepsilon s + 1)}}. \tag{16}$$

By analyzing the equivalent circuits in Figures 5 and 6, the various input–output expressions of the actuator were obtained. These coupling equations were found by using the voltage–current relationship of an ideal linear transformer and the method of circuit analysis [21]. The mesh-current method was used to analyze the voltage–current relationship in the ideal linear transformer model, the variables in the circuit were described in Figure 5, and the relationship between the mesh current equation and the voltage–current is as follows:

$$\begin{cases} u = R_{dc}(i - i_1) \\ u = i_1 Z_p + u_1 \\ F = Z_{m2}\dot{y} + Z_{m1}(\dot{y} - \dot{y}_1) \\ F_1 + Z_{m1}(\dot{y}_1 - \dot{y}) = 0 \\ \dot{y}_1 = -Ni_1 \\ F_1 = \dfrac{1}{N} \cdot u_1 \end{cases}. \tag{17}$$

The intermediate variables i_1, u_1, F_1, and $\dot{y}_1$ in Equation (17) were eliminated and the system of linear coupling equations was solved to obtain as follows:

$$\begin{cases} u = \dfrac{R_{dc}\left(N^2 Z_{m1} + Z_p\right)}{R_{dc} + N^2 Z_{m1} + Z_p} \cdot i + \dfrac{NR_{dc}Z_{m1}}{R_{dc} + N^2 Z_{m1} + Z_p} \cdot \dot{y} \\ F = \dfrac{NR_{dc}Z_{m1}}{R_{dc} + N^2 Z_{m1} + Z_p} \cdot i + \dfrac{\left(R_{dc} + Z_p\right) \cdot (Z_{m1} + Z_{m2}) + N^2 Z_{m1} Z_{m2}}{R_{dc} + N^2 Z_{m1} + Z_p} \cdot \dot{y} \end{cases}. \tag{18}$$

Rewriting Equation (18) in matrix form:

$$\begin{bmatrix} u \\ F \end{bmatrix} = \begin{bmatrix} \dfrac{R_{dc}\left(N^2 Z_{m1} + Z_p\right)}{R_{dc} + N^2 Z_{m1} + Z_p} & \dfrac{NR_{dc}Z_{m1}}{R_{dc} + N^2 Z_{m1} + Z_p} \\ \dfrac{NR_{dc}Z_{m1}}{R_{dc} + N^2 Z_{m1} + Z_p} & \dfrac{\left(R_{dc} + Z_p\right) \cdot (Z_{m1} + Z_{m2}) + N^2 Z_{m1} Z_{m2}}{R_{dc} + N^2 Z_{m1} + Z_p} \end{bmatrix} \cdot \begin{bmatrix} i \\ \dot{y} \end{bmatrix}. \tag{19}$$

Assuming that the reflected impedance of the transformer is negligible compared to the electrical impedance Z_p, the coefficient matrix in Equation (19) can be simplified. Based on whether the right end of the circuit is an open circuit, the reflected impedance of the transformer has different expression forms, mainly divided into two cases: (1) Clamping boundary conditions, where there is an external force, and the right end is an open circuit; (2) Free boundary conditions, that is, the external force is zero, and the right end is equivalent to a short circuit.

(1) Clamping boundary conditions:

$$N^2 Z_{m1} \ll Z_p. \tag{20}$$

(2) Free boundary conditions:

$$N^2 \cdot \frac{Z_{m1} Z_{m2}}{Z_{m1} + Z_{m2}} \ll Z_p. \tag{21}$$

Substituting Equations (20) and (21) into Equation (19), we obtain:

$$\begin{bmatrix} u \\ F \end{bmatrix} = \begin{bmatrix} \dfrac{R_{dc}Z_p}{R_{dc} + Z_p} & \dfrac{NR_{dc}Z_{m1}}{R_{dc} + Z_p} \\ \dfrac{NR_{dc}Z_{m1}}{R_{dc} + Z_p} & Z_{m1} + Z_{m2} \end{bmatrix} \cdot \begin{bmatrix} i \\ \dot{y} \end{bmatrix}. \tag{22}$$

If Z_p and R_{dc} satisfy the following relationship:

$$\left|\frac{Z_p}{R_{dc}}\right| \ll 1. \tag{23}$$

Then, Equation (22) can be further simplified as follows:

$$\begin{bmatrix} u \\ F \end{bmatrix} = \begin{bmatrix} Z_p & NZ_{m1} \\ NZ_{m1} & Z_{m1} + Z_{m2} \end{bmatrix} \cdot \begin{bmatrix} i \\ \dot{y} \end{bmatrix}. \tag{24}$$

Substituting Equations (10), (11), and (16) into Equation (24), the electromechanical coupling equation represented by the geometric parameters and material characteristic parameters of the ILG soft actuator is obtained as follows:

$$\begin{bmatrix} u \\ F \end{bmatrix} = \frac{1}{s} \begin{bmatrix} \dfrac{b}{Lw} \cdot \dfrac{1}{\varepsilon^T(s)} & \dfrac{3b^2}{4LL_F} \cdot \dfrac{dE}{\varepsilon^T(s)} \\ \dfrac{3b^2}{4LL_F} \cdot \dfrac{dE}{\varepsilon^T(s)} & \dfrac{Ewb^3}{4{L_F}^3} + s^2 \dfrac{3L_0^4 \rho_m wb}{{L_F}^3 \Gamma^4} \end{bmatrix} \cdot \begin{bmatrix} i \\ \dot{y} \end{bmatrix}. \tag{25}$$

3.2.2. Drive Equations. From the electromechanical coupling Equation (18) and the transformer reflection impedance assumptions Equations (20) and (21), the parameters of

each circuit component are represented with geometric parameters and material characteristic parameters of the soft actuator. The input–output relationship expression for the soft actuator represented by the geometric parameters and material characteristic parameters was obtained. According to the actuator input and output transfer function, the drive performance of the soft actuator with specific geometric parameters and material characteristic parameters can be determined easily. The driving equations for the actuator were solved with the end clamping boundary condition and the end free boundary condition.

(1) End clamping boundary conditions:

When $\dot{y} = 0$, the expression for the relationship between the clamping force and the input voltage was obtained by the solution to Equation (25) as follows:

$$\frac{F}{u}\Big|_{\dot{y}=0} = \frac{NZ_{m1}}{Z_p} = \frac{3dbwE}{4L_F}. \tag{26}$$

Similarly, the expression for the relationship between the clamping force and the input current is as follows:

$$\frac{F}{i}\Big|_{\dot{y}=0} = NZ_{m1} = \frac{1}{s}\frac{3db^2E}{4L_FL\varepsilon^T(s)}. \tag{27}$$

(2) End-free boundary conditions:

The clamping force was set to $F = 0$ in Equation (18), and we obtain:

$$\frac{y}{u}\Big|_{F=0} = \left[NZ_{m1} - \frac{Z_p(Z_{m1} + Z_{m2})}{NZ_{m1}}\right]\dot{y}. \tag{28}$$

From the impedance transformation condition (20), it can be seen that $NZ_{m1} \ll \frac{Z_p}{N}$, substituting it into Equation (28), integrating in the s domain and ignoring the inertia term Z_{m2}, the relationship between the displacement at the end of the actuator and the input voltage is as follows:

$$\frac{y}{u}\Big|_{F=0} = -\frac{N}{sZ_p} = -\frac{3dL_F^2}{b^2}. \tag{29}$$

4. Parameter Identification for the Soft Actuator Model

The soft actuator sample size was 35 mm × 5 mm × 0.5 mm, the free segment length was 30 mm, the average thickness of the activated carbon electrode layer was approximately 0.05 mm, and the average thickness of the ILG layer was approximately 0.4 mm. Before testing, the upper end of the sample was clamped vertically and fixed on the operating platform, and the lower end was free. The excitation signal was a step signal with an amplitude of 4 V. To accurately measure the displacement at the end of the soft actuator, a coordinate paper with 1 mm × 1 mm grid sizes was placed on the bracket behind the actuator. The coordinate paper was used to indicate the swing running displacement after the actuator was energized. The complete motion of a soft actuator was shot and recorded synchronously with a digital camera. The frame rate of the camera was 25 fps, and the swing displacement data were read every 2 s. To obtain stable test data, the actuator was run for three cycles with a square wave signal with an amplitude of 4 V, a period of 30 s, and a duty cycle of 50% before formal testing.

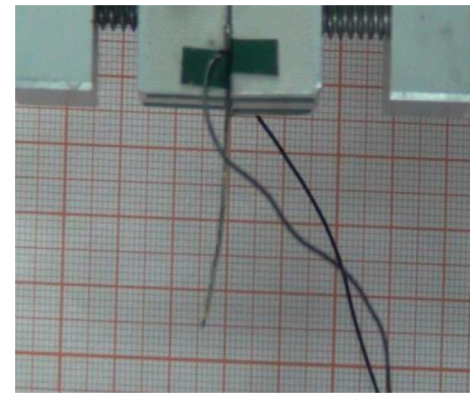

Figure 7: Soft actuator displacement captured with a digital camera at $t = 60$ s.

The computer sent an excitation control signal to the soft actuator through an electrochemical workstation. The positive and negative directions of the applied voltage are shown in Figure 7, and the left voltage was positive, and the right voltage was negative. The VideoReader function of MATLAB software was used to read the video shot by the digital camera. Combined with the video frame rate, the transient motion image of the actuator was captured and saved, and each frame of the video was read. According to the reference coordinate paper in the image, the horizontal displacement of the end of the actuator from the mid-perpendicular line (reference zero point) at that moment can be read and recorded. The left swing of the actuator was negative, and the right swing was positive.

Figure 7 shows a screenshot of the bending deformation displacement of the soft actuator at $t = 60$ s from the video taken with the digital camera, and the end displacement of the actuator was read after enlarging the picture. With an accuracy of 0.1 mm, the displacement at $t = 55$ s was approximately 4.6 mm, and the displacement of the actuator at this moment was the maximum value for the whole motion process. Screenshots of the soft actuator during bending deformations are shown in Figure 8. The complete horizontal displacement–time curve for the end of the actuator is shown in Figure 9, and the horizontal displacement at the end of the actuator was basically stable after 80 s. The horizontal displacement fluctuated within the range 4.2 ± 0.1 mm due to the accuracy of the coordinate paper.

4.1. Parameter Identification of the Equivalent Circuit Model. The current–time response curve recorded by the soft actuator electrochemical workstation is shown in Figure 10.

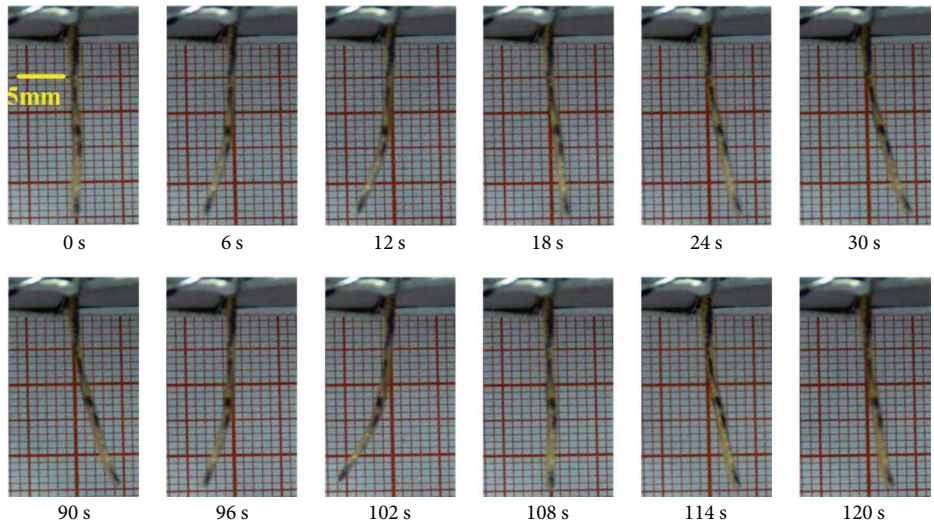

Figure 8: Screenshots of the soft actuator during bending deformations.

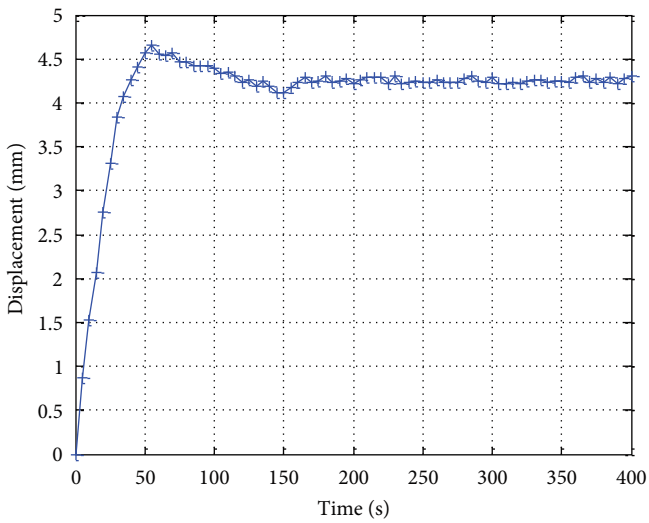

Figure 9: Step response of the soft actuator.

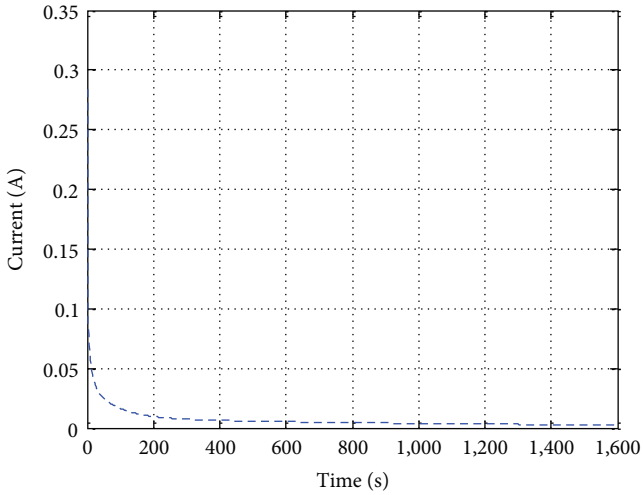

Figure 10: Step response curve for the soft actuator.

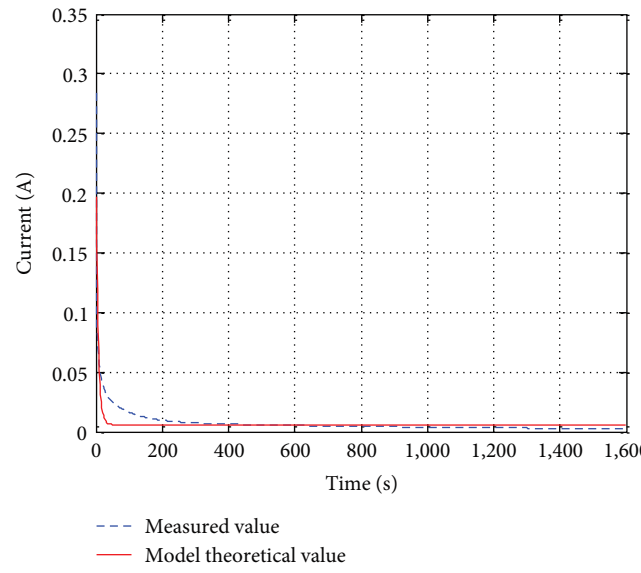

Figure 11: Comparison of soft actuator current response curves.

The lsqcurvefit function in MATLAB software was used to fit the step response curve of the soft actuator with the nonlinear least-squares method, and the optimal parameters obtained were $a_0 = 0.0060$, $a_1 = 0.2058$, and $\lambda = 0.1470$. With the 4 V step voltage input signal, the response of the current fitted by the driver is as follows:

$$i(t) = 0.006 + 0.2058e^{-0.147t}. \tag{30}$$

The soft actuator current–time simulation curve and the measured current response curve are shown in Figure 11; the fitting effects of the model in the initial stage and the steady-state process were good, but the deviation in the middle section (50–150 s) was large. The fitting accuracy J_1 was 0.0362, and the overall fitting result was basically satisfactory. The experimental data show that the current response of the

Table 1: Soft actuator geometry/circuit element parameters.

Static resistance, R_{dc} (Ω)	Dynamic resistance, R_d (Ω)	Capacitance, C (F)	Total length, L (cm)	The length of the dangling segment, L_0 (cm)	Width, w (cm)	Total thickness, b (mm)
667.6667	19.4363	0.3499	3.5	3	0.5	0.5

ILG soft actuator took a long time to reach the steady state, which was approximately 300 s. However, the steady-state times of the current responses for traditional IPMC materials are approximately a few seconds to tens of seconds [22]. This is because the viscosities of the ILG actuator ionic liquids are much greater than those of the aqueous solutions, resulting in slower migration of free ions under an applied electric field, so the time required to reach a steady state was longer.

4.2. Parameter Identification for the Actuator Mechanical System Model. The characteristic electrical parameters, such as the resistivity and permittivity, of the soft actuator material are shown in Table 1. The static/dynamic resistivity and permittivity of the soft actuator are shown in Table 2.

Referring to the optimal form of the piezoelectric coupling coefficient, the electromechanical coupling coefficient d of the soft actuator can be described by the following equation [23]:

$$d = K_d \frac{s + Z_d}{s^2 + 2\varsigma' \omega_n' s + \omega_n'^2}. \tag{31}$$

With the free boundary condition at the end of the soft actuator, Equation (31) was substituted into Equation (29) to obtain:

$$\frac{y}{u}\Big|_{F=0} = -\frac{3L_F^2 K_d}{b^2} \cdot \frac{s + Z_d}{s^2 + 2\varsigma' \omega_n' s + \omega_n'^2}. \tag{32}$$

When the excitation voltage was a step signal with amplitude U ($u = \frac{U}{s}$), it was obtained from Equation (32) as follows:

$$y = -\frac{3L_F^2 K_d V}{b^2} \cdot \frac{s + Z_d}{s(s^2 + 2\varsigma' \omega_n' s + \omega_n'^2)}. \tag{33}$$

The inverse Laplace transformation was performed on both sides of Equation (33) to solve for the deflection expression in the time domain: as follows:

$$y(t) = -\frac{3UL_F^2 K_d}{b^2} \cdot \left[\frac{Z_d}{\omega_n'^2} - \frac{Z_d}{\omega_n'^2} e^{-\varsigma' \omega_n' t} \cos\left(\omega_n' \sqrt{1 - \varsigma'^2} t\right) - \frac{Z_d \varsigma' - \omega_n'}{\omega_n'^2 \sqrt{1 - \varsigma'^2}} e^{-\varsigma' \omega_n' t} \sin\left(\omega_n' \sqrt{1 - \varsigma'^2} t\right)\right]. \tag{34}$$

The displacement response of the soft actuator to the 4 V step voltage signal is shown in Figure 8, where $U = 4$ V, $b = 0.5$ mm, and $L_F = L_0 = 30$ mm. The lsqcurvefit function in MATLAB was used to provide a nonlinear least squares fit for the actuator step response curve. The optimal values of each parameter in Equation (31) are shown in Table 3, and the time-domain expression for the end displacement (deflection) of the soft actuator was solved by substituting those values into Equation (34) as follows:

Table 2: Soft actuator characteristic parameters.

Static resistivity, ρ_{dc} (Ω·m)	Dynamic resistivity, ρ_d (Ω·m)	Permittivity, ε ($F \cdot m^{-1}$)
23.3683	0.6803	9.9971

Table 3: Electromechanical coupling parameters of the soft actuator.

K_d	Z_d	ς'	ω_n'
2.4448×10^{-6}	0.2075	0.6212	0.0742

$$y(t) = 3.9805 - 3.9805e^{-0.0461t}\cos 0.0581t - 1.3392e^{-0.0461t}\sin 0.0581t. \tag{35}$$

5. Effects of the Structural Parameters on the Performance of Soft Actuators

5.1. Influence of the Structural Parameters of the Soft Actuator on the Displacement at the End of the Actuator. Under the action of the step driving voltage, the electromechanical coupling parameters of the actuator identified in Table 3 were substituted into Equation (34), and the time-domain expression of the end displacement of the soft actuator is as follows:

$$y(t) = -\frac{UL_0^2}{b^2} \cdot 7.3344 \times 10^{-6} \cdot [37.6902 - 37.6902e^{-0.0461t}\cos 0.0581t - 12.6801e^{-0.0461t}\sin 0.0581t]. \tag{36}$$

The steady-state value is as follows:

$$y(\infty) = -\frac{UL_0^2}{b^2} \cdot 2.7644 \times 10^{-4}. \tag{37}$$

When the amplitude of the input step voltage was $U = 4$ V, the relationship between the end displacement of the robot and the length and thickness of the free end of the

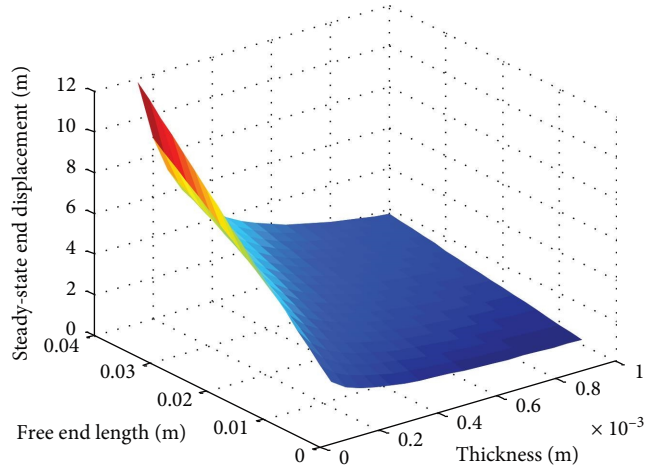

Figure 12: Relationships between the end displacement of the robot and the length and thickness of the actuator.

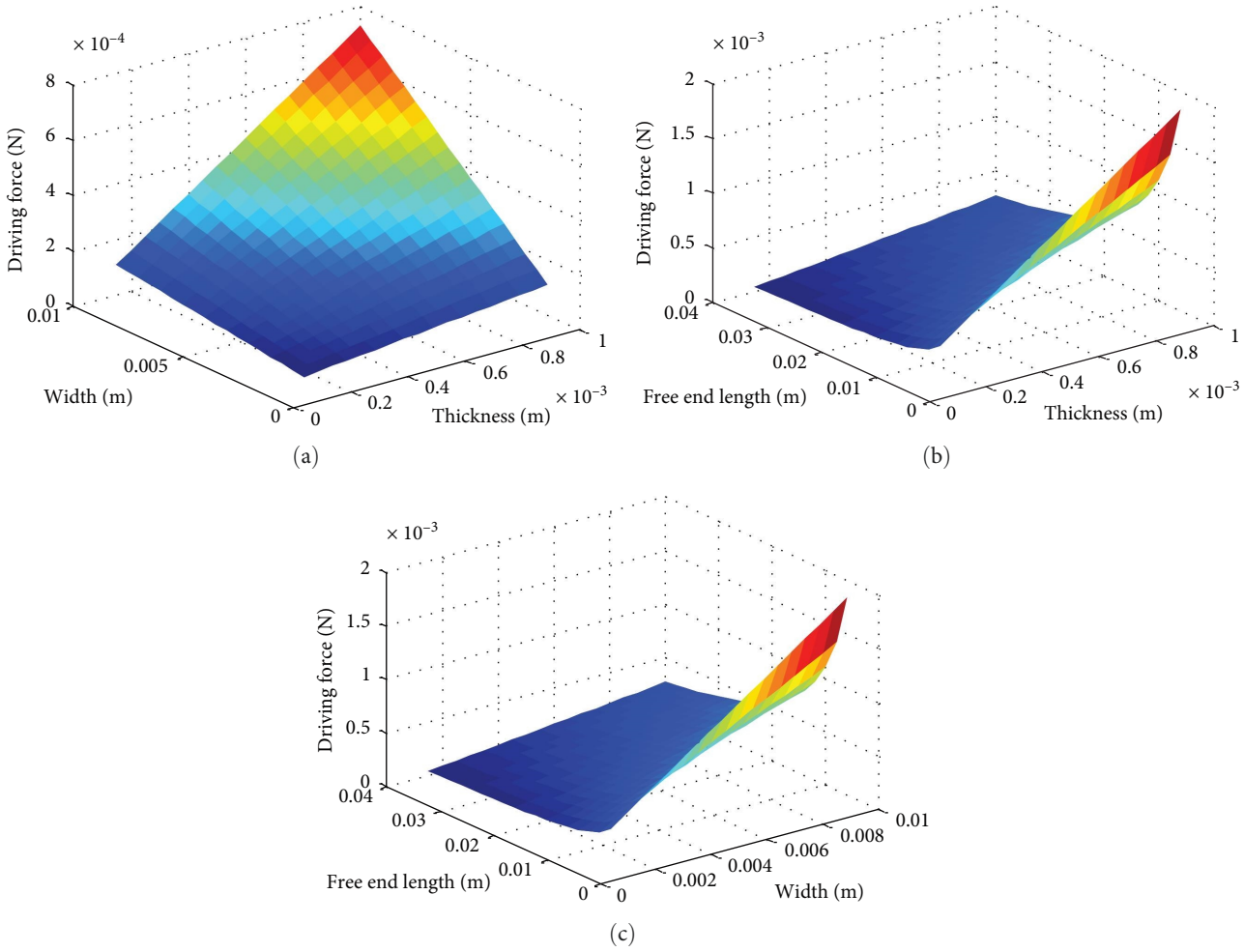

Figure 13: Relationships between the steady-state driving force of the robot and the length, thickness, and width of the free end of the actuator. (a) Actuator $L_0 = 30$ mm. (b) Actuator $w = 5$ mm. (c) Actuator thickness $b = 0.5$ mm.

actuator was as shown in Figure 12. Equation (37) shows that the theoretical displacement of the actuator was proportional to the square of the ratio of the length to the thickness of the free end but was independent of the actuator width. Theoretically, the increased actuator width was equivalent to a parallel arrangement of multiple narrow actuators, and the movements of each soft actuator were independent of each other, so the end displacement of the soft actuator was the same.

5.2. Influence of the Soft Actuator Structural Parameters on the Driving Force of the Actuator. The elastic modulus of the ILG material was $E = 7.6$ kPa, which was used as the equivalent elastic modulus of the soft actuator because the activated carbon layer was relatively thin. From Equation (26), the time-domain expression for the driving force of the soft actuator under the action of the step voltage is as follows:

$$F(t) = \frac{Ubw}{L_0} \cdot 1.4632 \times 10^{-2} \cdot \left[37.6902 - 37.6902e^{-0.0461t}\cos 0.0581t - 12.6801e^{-0.0461t}\sin 0.0581t\right]. \tag{38}$$

The steady-state value is as follows:

$$F(\infty) = \frac{0.5515Ubw}{L_0}. \tag{39}$$

When the input step voltage amplitude is $U = 4$ V, the relationship between the steady-state driving force of the robot and the length, thickness and width of the free end of the actuator is as shown in Figure 13. From Equation (39) the steady-state driving force of the soft robot was directly proportional to the thickness and width of the actuator and inversely proportional to the length of the free end of the actuator. At present, due to the large specific gravities of the ionic liquids contained in ILG and the small elastic modulus of the actuator, the driving force of the soft actuator is theoretically small.

It should be pointed out that the above model was established without considering the influence of gravity of an ILG soft body actuator and was equivalent to a slender cantilever beam structure. Therefore, whether the relationships among the length, thickness, and width of the soft actuator make their own gravity cannot be ignored, and it is necessary to determine the scope for application of the soft actuator model through the experimental research.

6. Conclusion

In this paper, the electromechanical coupling model of an ILG soft actuator was studied in depth, and a complete modeling idea was proposed, which provided a theoretical basis for the design of ILG soft robot mechanisms and control methods. Based on the IPMC actuator electrical model proposed by Claudia Bonomo, combined with the characteristics of ILG materials, the current of the actuator was classified. In describing the steady-state characteristics/dynamic characteristics of the actuator, a suitable simplified *R–C* equivalent circuit model was established. The equivalent circuit described the relationship between the input voltage and the response current of the actuator. Drawing on the modeling ideas of supercapacitors, an equivalent circuit model of an ILG soft actuator was developed. The time/frequency domain response of the current was derived by using the basic principle of the circuit and Laplace transform method. The theoretical simulation and experimental current curve under the action of step voltage were compared. The parameters of each circuit component in the equivalent circuit model were identified with the least squares method.

The electromechanical coupling gray box model of the actuator was established. Combined with the Laplace transform, the electromechanical coupling equation system of the actuator was derived while considering the structural parameters of the actuator. Then, the correspondence between the input and output variables of the system was given. The influence of geometric parameters/material characteristic parameters of the actuator on the displacement and driving force at the end of the actuator is described. The least-squares method was used to identify the system parameters. The simulation results showed that the established electromechanical coupling gray box model simulated the electromechanical conversion characteristics of the actuator effectively. The electromechanical coupling gray box model combining geometric parameters/material showed a better fit and higher accuracy for ILG soft actuators.

Finally, a series of experiments was used to identify the model parameters, and the effectiveness of the model was verified from different perspectives. The experimental results showed that the model had good accuracy and versatility and can be used for robot actuator mechanism design and control algorithm research.

Data Availability

The data used to support the findings of this study are included within the article.

Conflicts of Interest

The authors declare that they have no conflicts of interest regarding the publication of this paper.

Acknowledgments

This work was supported by Joint Open Fund of the Guizhou Provincial Department of Education (grant no. [2022] 439), the Science and Technology Research Project of Henan Province, China (grant no. 222102220022), the Doctoral Research Foundation of Guiyang University, China (grant no. GYU-KY-2023), and the Guizhou Provincial Basic Research Program (Natural Science) (grant no. ZK [2023] 011).

References

[1] X. Hao, H. Wenren, X. Wang, X. Xia, and J. Tu, "A gel polymer electrolyte based on PVDF-HFP modified double polymer matrices via ultraviolet polymerization for lithium-sulfur batteries," *Journal of Colloid and Interface Science*, vol. 558, pp. 145–154, 2020.

[2] B. He, C. Zhang, Y. Zhou, and Z. Wang, "A computing method to determine the performance of an ionic liquid gel soft actuator," *Applied Bionics and Biomechanics*, vol. 2018, Article ID 8327867, 11 pages, 2018.

[3] S. Saito, Y. Katoh, H. Kokubo, M. Watanabe, and S. Maruo, "Development of a soft actuator using a photocurable ionic gel," *Journal of Micromechanics and Microengineering*, vol. 19, no. 3, Article ID 035005, 2009.

[4] F. Guo, T. Sun, P. Wang, S. Liu, B. Lian, and Y. Song, "Multistability of a planar three-limb flexible mechanism," *Mechanism and Machine Theory*, vol. 175, Article ID 104956, 2022.
[5] J. Zhao, X. Wang, C. Meng, H. Song, Z. Luo, and Q. Han, "Dynamic modeling and analysis of thrust reverser mechanism considering clearance joints and flexible component," *Aerospace*, vol. 9, no. 10, Article ID 611, 2022.
[6] M. Su, Y. Zhang, H. Chen, Y. Guan, and C. Xiang, "Modeling, analysis, and computational design of muscle-driven soft robots," *Soft Robotics*, vol. 10, no. 4, pp. 808–824, 2023.
[7] Z. Yu, H. Peiyu, Y. Bo, Y. Zhibin, L. Dongjie, and D. Guoqi, "Design and motion simulation of a soft robot for crawling in pipes," *Applied Bionics and Biomechanics*, vol. 2023, Article ID 5334604, 8 pages, 2023.
[8] D. Wang, J. Wang, Z. Shen et al., "Soft actuators and robots enabled by additive manufacturing," *Annual Review of Control, Robotics, and Autonomous Systems*, vol. 6, no. 1, pp. 31–63, 2023.
[9] Z. Ma and D. Sameoto, "A review of electrically driven soft actuators for soft robotics," *Micromachines*, vol. 13, no. 11, Article ID 1881, 2022.
[10] D. Li, D. Fan, R. Zhu et al., "Origami-inspired soft twisting actuator," *Soft Robotics*, vol. 10, no. 2, pp. 395–409, 2023.
[11] J. Asada, N. Usami, H. Ota, M. Watanabe, and K. Ueno, "Liquid metal-ionic liquid composite gels for soft, mixed electronic-ionic conductors," *Macromolecular Chemistry and Physics*, vol. 223, no. 8, Article ID 2100319, 2022.
[12] F. C. Tavares, C. M. Cholant, E. C. Kohlrausch et al., "Ionic liquid boosted conductivity of biopolymer gel electrolyte," *Journal of the Electrochemical Society*, vol. 170, no. 8, Article ID 084501, 2023.
[13] M. Annabestani, N. Naghavi, and M. Maymandi-Nejad, "From modeling to implementation of a method for restraining back relaxation in ionic polymer–metal composite soft actuators," *Journal of Intelligent Material Systems and Structures*, vol. 29, no. 15, pp. 3124–3135, 2018.
[14] Q. He, G. Yin, D. Vokoun et al., "Review on improvement, modeling, and application of ionic polymer metal composite artificial muscle," *Journal of Bionic Engineering*, vol. 19, no. 2, pp. 279–298, 2022.
[15] Q. Yao, G. Alici, and G. M. Spinks, "Feedback control of trilayer polymer actuators to improve their positioning ability and speed of response," *Sensors and Actuators A: Physical*, vol. 144, no. 1, pp. 176–184, 2008.
[16] X. Liu, B. He, Z. Wang, H. Tang, T. Su, and Q. Wang, "Tough nanocomposite ionogel-based actuator exhibits robust performance," *Scientific Reports*, vol. 4, no. 1, Article ID 6673, 2014.
[17] C. Zhang, B. He, Z. Wang, Y. Zhou, and A. Ming, "Application and analysis of an ionic liquid gel in a soft robot," *Advances in Materials Science and Engineering*, vol. 2019, Article ID 2857282, 14 pages, 2019.
[18] G. Selleri, F. Poli, R. Neri et al., "Energy harvesting and storage with ceramic piezoelectric transducers coupled with an ionic liquid-based supercapacitor," *Journal of Energy Storage*, vol. 60, Article ID 106660, 2023.
[19] C. Zhang, B. He, A. Ding, S. Xu, Z. Wang, and Y. Zhou, "Motion simulation of ionic liquid gel soft actuators based on CPG control," *Computational Intelligence and Neuroscience*, vol. 2019, Article ID 8256723, 11 pages, 2019.
[20] K. M. Newbury and D. J. Leo, "Linear electromechanical model of ionic polymer Transducers-Part I: model development," *Journal of Intelligent Material Systems and Structures*, vol. 14, no. 6, pp. 333–342, 2003.
[21] H.-L. Xing, J.-H. Jeon, K. C. Park, and I.-K. Oh, "Active disturbance rejection control for precise position tracking of ionic polymer–metal composite actuators," *IEEE/ASME Transactions on Mechatronics*, vol. 18, no. 1, pp. 86–95, 2013.
[22] L. Napollion and K. J. Kim, "Electrochemical performance of ionic polymer metal composite under tensile loading," *Smart Materials and Structures*, vol. 32, no. 9, Article ID 095025, 2023.
[23] C. Bonomo, L. Fortuna, P. Giannone, S. Graziani, and S. Strazzeri, "A nonlinear model for ionic polymer metal composites as actuators," *Smart Materials and Structures*, vol. 16, no. 1, pp. 1–12, 2007.